Energy harvesting from galloping of prisms: A wind tunnel experiment

Pascal Hémon[a,*], Xavier Amandolese[a,b], Thomas Andrianne[c]

[a] LadHyX, Ecole Polytechnique – CNRS, 91128 Palaiseau Cédex, France
[b] Conservatoire National des Arts et Métiers, Paris, France
[c] Aerospace and Mechanical Engineering Department, University of Liège, Allée de la Découverte, 9 Quartier Polytech 1, B52/3, 1, Liège 4000, Belgium

ARTICLE INFO

ABSTRACT

We study the energy harvesting from the galloping oscillations of rigid prisms flexibly mounted in a wind tunnel. A square section and a 2/3 rectangular section are tested and the inclination angle of the prisms referred to the flow direction is optimally adapted. The energy harvester is based on magnets moving with the prism in the front of a coil-core at rest. Energy is dissipated in a load resistance for which an optimal value is found. Efficiency of the "prism wind turbine" is weak compared to usual wind turbine due to the physics of the galloping mechanism. However such systems remain interesting for their potential of adaptation to various situations.

1. Introduction

Galloping is a dynamic instability affecting slender structures submitted to a cross flow. It is generally referred to be a one degree of freedom instability, in transverse or torsional motion, for which the motion-induced fluid loading creates a negative added damping that can trig the instability beyond a critical velocity (Païdoussis et al., 2011). As pointed out by Blevins (2001), slender structures with non-circular bluff cross sections are all susceptible to transverse galloping. It is then a matter of great concern in civil and offshore engineering for which bluff structures are submitted to wind and/or water current. Recently the idea emerged that the galloping phenomenon could be used for designing an energy harvester from wind or water current.

The literature on transverse galloping is important and one can find the most significant references in the book of Blevins (2001), the paper of Parkinson (1989) and the recent book of Païdoussis et al. (2011). Energy harvesting from transverse galloping has been previously studied analytically by Barrero-Gil et al. (2010) and Vicente-Ludlam et al. (2014). In the latter, an energy harvesting device model is coupled with a simple galloping non-linear model. Recently, Kiwata et al. (2016) used various cantilevered prisms in a water channel in order to extract energy with a iron-gallium alloy setup. They found that the global efficiency is very small with a maximum of 0.045%, which is much lower than the analytical results proposed by Vicente-Ludlam et al. (2014).

In that context, the objective of this paper is to evaluate and discuss the energy harvesting potential of the galloping mechanism in air with square and rectangular prisms. Although square and rectangular sections may not be the most efficient shapes for harvesting energy, this experimental contribution could allow to improve the mathematical models and assess the performances from a wind engineering point of view.

The paper is organized as follows: after a short review of galloping, the experimental methodology regarding the measurements, galloping section model set-up, and energy harvesting methodology are presented in Section 3. Galloping results and energy

---

* Corresponding author.
E-mail address: pascal.hemon@ladhyx.polytechnique.fr (P. Hémon).

Nomenclature		R_L	coil resistance (Ω)
		Re	Reynolds number
A	non dimensional response amplitude of the prism (RMS), $A = Z_{RMS}/D$	S	span of the prism (m)
		S_c	Scruton number, $S_c = 2m\eta/\rho BD$
B, D	dimensions of the prism section (m)	U	mean velocity (m/s)
C_l, C_d	lift and drag coefficients	U_a	apparent velocity (m/s)
C_Z	transverse force coefficient	U_c	critical velocity (m/s)
C_Z'	derivative of transverse force coefficient (rad^{-1})	U_r	reduced velocity, $U_r = U/fD$
F_Z	aerodynamic transverse force on the prism (N)	$V(t)$	load voltage (V)
f	natural frequency of motion (Hz)	$Z(t)$	vertical displacement of the prism (m)
k	stiffness of the elastically supported prism (N/m)	θ_0	rotation angle of the prism (°)
k_E	electromechanical coupling coefficient	μ	efficiency (%)
L	inductance of the energy harvester (H)	η	reduced structural damping, referred to critical damping (%)
M	total mass of the prism (kg)		
m	mass per unit length of the prism (kg/m), $m = M/S$	η_a	reduced aerodynamic damping, referred to critical damping (%)
P_e	electric power (W)	η_E	reduced electromechanical damping, referred to critical damping (%)
P_g	maximum power available by galloping oscillations (W)		
P_w	wind power (W)	ρ	air density (kg/m^3)
R	load resistance (Ω)	ω	angular frequency of motion (rad/s)

harvesting results are reported in Section 4. Finally, energy harvesting efficiencies are discussed in Section 5.

2. Short review of the galloping phenomenon

The basic mechanism of transverse galloping was first analysed by Den Hartog in 1934 (Den Hartog, 1985), in the context of transmission line vibration when sleet is found on the wire. In his pioneer work, Den Hartog proposed a quasi-static criterion for the onset of this damping driven instability. It is briefly recalled here, following the presentation of Novak (1969) and Blevins (2001) and considering the section model notation that is used in the present study.

Consider a prismatic cross section, Fig. 1, flexibly mounted in order to allow a single degree of freedom motion, Z(t), perpendicularly to a steady flow characterized by a velocity U. The equation of motion is given by (1)

$$\ddot{Z} + 2\omega\eta\dot{Z} + \omega^2 Z = \frac{1}{M}F_Z, \tag{1}$$

where M is the mass of the prism, ω its natural frequency, η its damping ratio due to dissipation in the spring-supported setup and F_Z is the transverse aerodynamic force.

Assuming that the fluid force acting on the system is quasi-static, *i.e.* function of the instantaneous apparent velocity seen by the prism, one can express F_z as

$$F_Z = \frac{1}{2}\rho U_a^2 SD \left[C_l(\theta_0 + \theta)\cos\theta + C_d(\theta_0 + \theta)\sin\theta \right], \tag{2}$$

where the apparent velocity is the sum of the cross flow velocity and the motion-induced velocity. Its square value and relative angle of attack θ are then defined as

$$U_a^2 = U^2 + \dot{Z}^2 \quad \text{and} \quad \theta = \tan^{-1}(-\dot{Z}/U). \tag{3}$$

In Eq. (2) ρ is the fluid density, C_l and C_d are the lift and drag force coefficient in and transverse to the direction of the
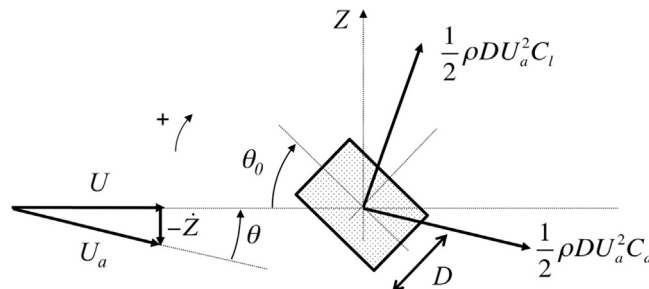

Fig. 1. Cross-section galloping model for one-degree-of-freedom transverse motion.

instantaneous apparent velocity, θ_0 is the angle of orientation of the cross section relative to the mean flow velocity and D is the transverse characteristic dimension of the prism, *i.e.* its "height" for $\theta_0=0°$. The choice of D, instead of B, as the reference length is motivated by the energy harvesting purpose of the paper for which the area normal to the flow is commonly used.

Introducing a transverse force coefficient $C_Z=F_Z/(0.5\rho U^2 SD)$, one finds:

$$C_Z(\theta_0, \theta)=\frac{U_a^2}{U^2}[C_l(\theta_0+\theta)\cos\theta+C_d(\theta_0+\theta)\sin\theta],$$ (4a)

which can be rewritten as follows

$$C_Z(\theta_0, \theta)=[C_l(\theta_0+\theta)+C_d(\theta_0+\theta)\tan\theta]\sec\theta.$$ (4b)

After linearization of the fluid force, the linearized equation of motion becomes

$$\ddot{Z}+2\omega\left[\eta+\frac{\rho DU}{4m\omega}\left(\frac{dC_z}{d\theta}\right)_{\theta=\theta_0}\right]\dot{Z}+\omega^2 Z=0,$$ (5)

where

$$\left(\frac{dC_Z}{d\theta}\right)_{\theta=\theta_0}=\left(\frac{dC_l}{d\theta}\right)_{\theta=\theta_0}+C_{d\theta=\theta_0}.$$ (6)

This leads to the Den Hartog criterion, assessing that a section can be unstable in plunge for some given orientations θ_0 when the sum of the slope of the lift coefficient with the drag coefficient at θ_0 is negative. A galloping instability occurs above a critical velocity (7) of the flow, which is the result of a balance between the added aerodynamic damping and the structural damping.

$$U_c=\frac{-4\eta m\omega}{\rho D\left(\left(\frac{dC_l}{d\theta}\right)_{\theta=\theta_0}+C_{d\theta=\theta_0}\right)}.$$ (7)

This expression for the critical velocity is of great practical importance. Indeed the quasi-static approximation is generally valid for reduced velocity $U_r=U/fD > 20$ and one only needs lift and drag coefficients data from static wind tunnel measurements. A useful compilation of the transverse force coefficient slope value for various sections in smooth or turbulent flow can be found in Blevins (2001). Effects of upstream turbulence and prism corner shapes have been also studied by Saathoff and Melbourne (1999) and recently by Carassale et al. (2013).

Once the system is unstable, oscillations grow in amplitude up to limit-cycle oscillations (LCO) due to structural or aerodynamic nonlinearities. If one wants to study the post-critical behaviour it is then necessary to take into account the nonlinear evolution of the transverse fluid force. This was originally done by Parkinson and Brooks (1961), Parkinson and Smith (1964) and Novak (1969) using a nonlinear quasi-steady approach. Using polynomial approximation of the static transverse force coefficient evolution with the angle of attack they obtained diagrams of amplitude-velocity response in very good agreement with experiments for the cases of prisms of square, rectangular and D-section. They also showed that due to the nonlinear evolution of the transverse force coefficient, bifurcation and hysteretic behaviour might occur in the galloping response.

Later a number of studies were done on the nonlinear galloping behaviour. An interesting discussion on the bifurcation leading to galloping for the case of prisms of square and low aspect ratio rectangular sections can be found in Novak (1971, 1972). Effect of turbulence on galloping can also be found in Novak and Tanaka (1974) along with a collection of coefficients for the polynomial expansion of the transverse fluid force. The hysteretic behaviour in post-critical galloping is also a matter of concern. Following the work of Parkinson and Smith (1964), Luo et al. (2003) performed a numerical study focusing on the hysteresis oscillation for the case of a square prism at $\theta_0=0$. They confirmed that the hysteretic behaviour is due to the inflexion point in the transverse force coefficient curve. Moreover the use of a seventh-order polynomial expansion is found necessary and sufficient to catch this nonlinearity (Ng et al., 2005). The link between inflexion points and LCO hysteresis response was also recently scrutinized by Barrero-Gil et al. (2009). In another study, Andrianne and Dimitriadis (2014) showed that a fifth-order expansion is sufficient to capture the bifurcation behaviour of galloping.

3. Experimental setup

3.1. Wind tunnel and measurement techniques

Tests have been performed in an Eiffel open-loop wind tunnel with a square closed test section of 180 by 180 mm. The air inlet is equipped with honeycomb and thin grid so that the turbulence intensity is less than 1% in the test section. The mean velocity can be varied from 4 to 25 m/s by means of a centrifugal fan. The reference velocity is measured via a Pitot tube and a Furness pressure transmitter. Air density is corrected by measurement of the air temperature in the wind tunnel with a thermocouple and the atmospheric pressure with a mercury barometer. The prisms generate a blockage effect (9.5% for the square section and 7% for the rectangular one) in the wind tunnel. Therefore a correction is applied on the reference velocity of the wind tunnel: it consists in increasing velocity by the blockage ratio, in order to keep the flow rate constant upstream and along the prism. No other correction was applied. Global accuracy of the reference velocity measurement is considered better than 1%.

Data acquisition is performed using a PAK system furnished by Muller-BBM. It is based on a 8 channels analyzer with 24 bits of resolution and sampling frequencies up to 52 kHz. This system provides time histories of the signal and simultaneous spectral analysis. Means and RMS values that are reported further are computed from at least 45 s of the history records sampled at 1024 Hz, which represents almost 250 periods of prisms oscillations. The final frequency resolution is 1/8 Hz.

3.2. Galloping setup

The prism models almost span the width of the test section. They are equipped with two end plates to keep the airflow as two-dimensional as possible. They are elastically supported in order to allow a one-degree-of-freedom transverse motion $Z(t)$. Stiffness is provided by combination of linear and laminated springs, suitably mounted in order to produce a very low structural damping. These springs are mounted outside the test section, via two vertical fences (see Fig. 2). Length of laminated springs is large (0.75 m) compared to the expected cylinder vertical displacement so that the system can be considered as linear in the range of use. The vertical displacement of the cylinder is measured by a laser sensor, *i.e.* without contact that could corrupt the damping of the system.

Structural parameters were identified under zero-wind velocity. A static weight calibration technique was used to measure the stiffness k of the setup. Free decay tests at small amplitude were performed to identify the natural angular frequency ω, by spectral analysis, and the damping ratio η, using a standard decrement technique. The total mass M of the system was then calculated using the measured stiffness and natural frequency and expressed as a mass per unit length, m, by dividing by the cylinder span.

For both configurations the Scruton number $S_c = 2m\eta/\rho BD$ is high and then the risk of vortex-induced vibration is expected to be very small. Moreover, in the reduced velocity range of the present study $U_r > 40$, estimated vortex shedding frequency (Norberg, 1993) is at least 6 time larger than the natural frequency of the prism so that any lock-in or interference possibility is moved away (Hémon, 2012; Mannini et al., 2014).

3.3. Prisms characteristics

Two prisms have been used in the present study. The first one has a square section of dimension D=17.1 mm and the second one has a rectangular section of ratio D/B=2/3 with D=12.3 mm, as shown Fig. 3. Both are made of aluminium alloy with a span S=170 mm. Their shape has been adjusted on a milling machine in order to produce corners with sharp edge. Their structural characteristics are given in Table 1. The damping ratio is measured from 10 decaying tests and the resulting scattering is mentioned between parenthesis. For the square section these structural parameters are independent of the angle θ_0.

Three series of tests have been made in order to study energy harvesting; two series with the square section for θ_0=0° and θ_0=10°
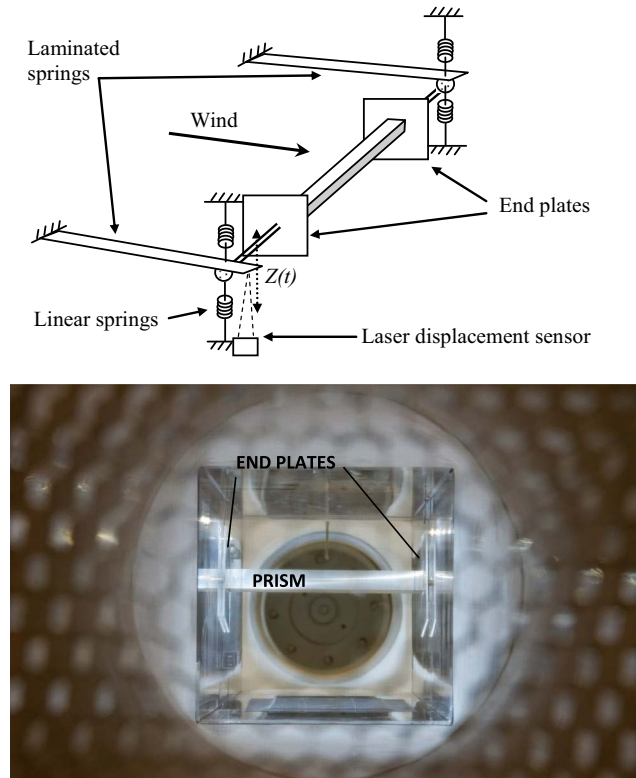

Fig. 2. Experimental setup schematic for galloping (top) and picture taken through the inlet of the wind tunnel (bottom).
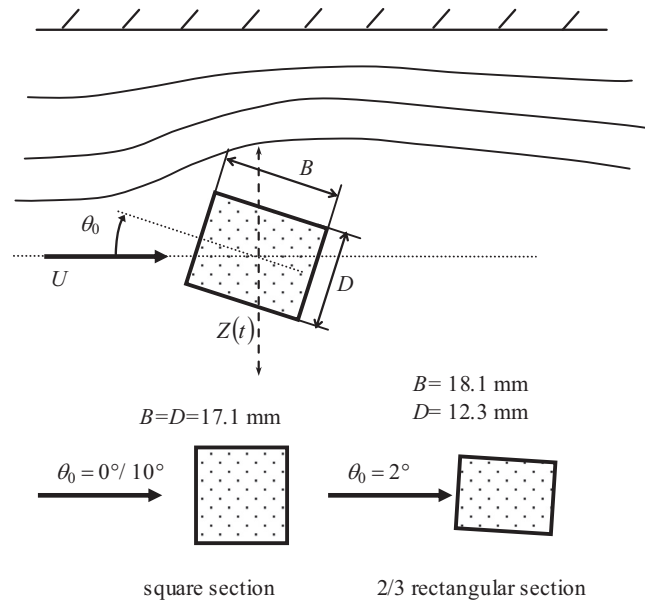
Fig. 3. Geometric details of the studied prisms and signs conventions.

and one series with the rectangular section for $\theta_0=2°$. These configurations are well known to be subject to galloping instability and they were chosen after preliminary observations because of the good stability of the limit cycle amplitudes.

Aerodynamic (drag and lift) and aeroelastic (flutter derivative) characteristics of the prisms are reported in Table 2. Measurements are performed in the same conditions than those encountered further, *i.e.* with the same prisms in the same range of Reynolds number and in the same wind tunnel. Drag and lift coefficients of the square section for $\theta_0=0°$ and $10°$ well agree with those of Parkinson and Brooks (1961) which are mentioned between parenthesis.

The flutter derivative term KH_1^* is particularly important in the galloping phenomenon (Païdoussis et al., 2011). It is associated to the velocity dependant term of the linear motion-induced transverse aerodynamic force. It is then similar to the transverse force derivative $dC_Z/d\theta$ in the quasi-steady limit. Here KH_1^* is measured dynamically as a growth rate of the amplitude of the prism motion, when the flow velocity is sufficiently high to generate galloping oscillations. For the square section at $\theta_0=0°$ it is possible to favourably compare the current result with the one of Novak (1969). These results are also consistent with those reported by Mannini et al. (2014). Particularly the values found here for the rectangular section at $\theta_0=2°$ are consistent with those given for $\theta_0=0°$.

3.4. Energy harvesting device

Different types of devices can be used to harvest the kinetic energy of a structure undergoing oscillations: piezoelectric, electrostatic (capacitive) or electromagnetic (inductive). Several theoretical and experimental researches have investigated piezo-electric technologies (Abdelkefi et al., 2013; Ewere et al., 2014; Michelin and Doaré, 2013; Sousa et al., 2011). Barrero-Gil et al. (2010) have studied the galloping instability, providing theoretical efficiency from the resulting vibrating motion. In another theoretical approach Vicente-Ludlam et al. (2014) used a simplified model of magnet/coil assembly to investigate the optimal energy harvesting strategy from a 2D galloping structure.

An electromagnetic system is used in the scope of this work. The proposed harvesting device consists in the combination of magnets in motion in the close vicinity of a coil and core static ensemble. The system is depicted in Fig. 4, where the variable load resistance is represented. The magnets are located on the suspension beams that ensure the vertical stiffness of the aeroelastic system.

The magnets combination is composed of three Neodymium magnets (NdFeB) of size $10×5×3$ mm, with a magnetization type N45. Attraction force of one magnet is 1.5 kg (data from supplier). The total mass of the magnets is equal to 3.33 g. It represents an

Table 1
Structural characteristics of the two prisms.

	Square	Rectangular
f (Hz)	5.88	5.75
M (kg)	0.340	0.326
η (%)	$0.19 ± 0.006$	$0.256 ± 0.009$
k (N/m)	467	425.5
S_c	21.4	36.7

Table 2
Measured aerodynamic and aeroelastic characteristics for the three configurations at *Re*=20000. Values between parenthesis are from Parkinson and Brooks (1961) and Novak (1969).

	Square θ_0=0°	Square θ_0=10°	Rectangular θ_0=2°
C_d	2.3 (2.35)	1.8 (1.8)	1.5
C_l	0.	−0.64 (−0.6)	−0.3
KH_1^*	−2.6 (−2.69)	−4.6	−5.3

increase of 1% of the total translating mass of the initial galloping system and induces an increase of the natural frequency lower than the measurement resolution (1/8 Hz). When the prism and the magnets are at rest or almost aligned in front of the coil-core, there is an influence on the structural damping ratio. Values given in Table 1 are measured at low motion amplitude and take into account this interference effect.

The dimensions of the coil are 22 mm long and 16 mm diameter. Measured inductance is L=0.0372 Henry and its electric resistance is R_L=37 Ω. The cylindrical core is 17 mm long and 6 mm diameter. The gap between magnets at rest and coil is 0.5 mm, which positions the core at 5.5 mm from the magnets. Due to the kinematics of the setup, with laminated springs, the magnets have a second order displacement which increases the gap of 0.3 mm maximum for the highest LCO amplitude reached in this study. The load resistance R of the harvesting device is adjustable between 0 Ω (short-circuit) up to 10^{10} Ω (open-circuit). A decade box from Time Electronics is used in the set-up. The load voltage $V(t)$ is measured synchronously with the vertical displacement $Z(t)$ using the PAK system.

The harvesting device is characterized through shaker tests. A sinusoidal motion of constant amplitude (Z_{rms}=7.2 mm) and frequency 5.75 Hz (see Table 1) is imposed to the magnets in front of the coil. The RMS voltage is measured for different values of the load resistance between 1 Ω and 9 MΩ. Fig. 5 shows that the maximum voltage is reached at 35 Ω. This value is close from the resistance of the coil (37 Ω), in accordance with the Maximum Power Transfer Theorem.

When electrical energy is extracted from a flow-induced moving body the global electrical efficiency of the harvesting system is classically defined by

$$\mu = P_e/P_w \tag{8}$$

which is the ratio of the electric power P_e with the wind power P_w. The electrical power output P_e of the harvesting device is calculated from the knowledge of the voltage and the load resistance

$$P_e = V_{RMS}^2/R \tag{9}$$

where V_{RMS} is the RMS of the measured voltage time history $V(t)$.

On the other hand, the wind power is defined as the kinetic energy flux of air passing throw a cross section defined by the area swept by the oscillating prism. It is the product of its span and thickness, increased by the measured amplitude oscillations, therefore:

$$P_w = \frac{1}{2}\rho S\left(D\cos\theta_0 + B\sin\theta_0 + 2 \; Z_{rms}\right)U^3 \tag{10}$$

which can be simplified for low values of θ_0:

$$P_w = \frac{1}{2}\rho S\left(D + 2 \; Z_{rms}\right)U^3. \tag{11}$$
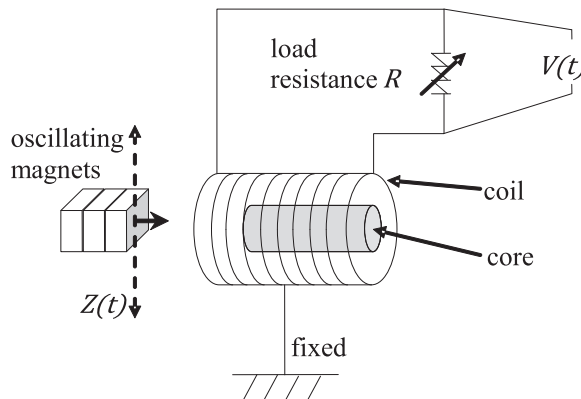
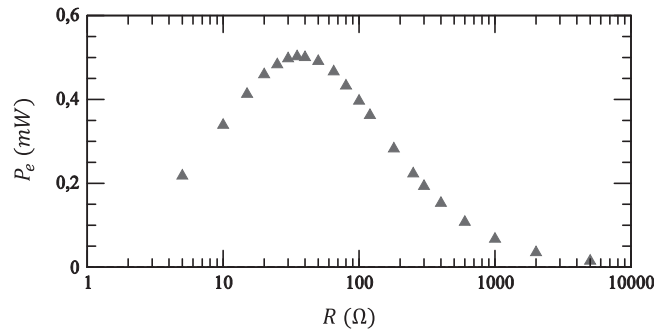**Fig. 4.** Principle of the electric energy harvesting device.

Fig. 5. Characterization of the harvesting device: electrical power output vs. load resistance.

4. Galloping and energy harvesting results

4.1. Galloping results without energy extraction

First of all the galloping response of the prisms is measured against the wind velocity in an open circuit configuration. The objective is to study the effect of the energy harvesting system without its electromechanical coupling. Measurements are performed with and without the core that may have an influence because of the magnets mounted just in front of it. In order to by-pass the additional damping produced when the magnets are almost aligned with the coil-core, all tests are performed by triggering manually the motion. Few millimeters of initial excitation are sufficient. Due to this initial excitation, only LCO amplitude with $A > 0.1$ are reported in the following results. Measurements for the square section are reported in Fig. 6 and in Fig. 7 for the rectangular section.

The non dimensional amplitude of the limit cycles is referred to the width D and computed from the RMS value of the record of $Z(t)$ once the system have reached a stable LCO regime. Results confirm that the influence of the core is small, even negligible. It means that the attractive electromechanical force between the magnets and the coil-core ensemble is sufficiently small not to disturb the galloping dynamics when the harvest is not activated (open loop circuit). In this study, with an air flow, the amplitudes reached by the LCO remain relatively small by comparison with similar experiments in water flow, so that only the first branch in the response curve described in Novak (1972) is concerned here.

4.2. Effect of the load resistance

The first series of tests are performed in order to study the influence of the energy harvesting at constant wind velocity. The wind speed is stabilized and the load resistance is decreased step by step, waiting each time the stability of the LCO in order to measure the efficiency and the associated non-dimensional amplitude of the LCO.

Results are depicted in Fig. 8 for the square section and Fig. 9 for the rectangular section. The global efficiency and the LCO amplitude are plotted versus the load resistance. It appears that the optimal resistance, for which the efficiency is maximum, is not constant and depends on the configuration: 90 Ω for the square section at $\theta_0=0°$, 48 Ω at $\theta_0=10°$ and 65–80 Ω for the rectangular section at $\theta_0=2°$.

Those results also show that the global efficiency of the system is very small, with a maximum value of 0.03% among the tested cases. These low efficiencies are consistent with those found by Kiwata et al. (2016) in their water channel experiment where they found a maximum of 0.045%. The difference between the two can be explained by the reference surface considered: in the present work it corresponds to the surface swept by the prism, while Kiwata et al. (2016) used the prism width.
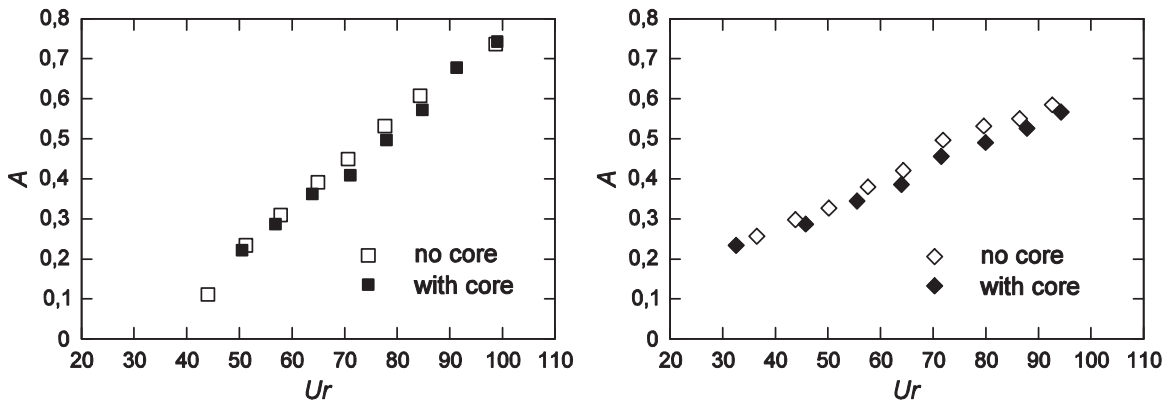

Fig. 6. Non dimensional galloping response ($A = Z_{RMS}/D$ vs U_r) of the square section without energy extraction (left: $\theta_0=0°$, right: $\theta_0=10°$).
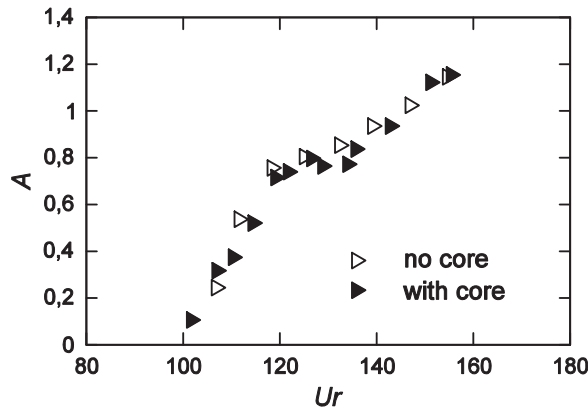
Fig. 7. Non dimensional galloping response ($A = Z_{RMS}/D$ vs U_r) of the rectangular section without energy extraction.

Regarding the effect of the load resistance on the LCO amplitude, results show that, starting from the free oscillations value for large load resistance, the amplitude remains almost constant by decreasing R, up to a region where the efficiency of the harvesting device becomes significant. By decreasing further the load resistance, an asymptotic value corresponding to the minimum resistance is reached. For the three configurations the maximum efficiency is obtained when the LCO amplitude reaches an intermediate value between the ones corresponding to the largest (open circuit) and the lowest (almost short-circuit) resistances. For the square section at $\theta_0 = 10°$, the difference of LCO amplitudes in those two extreme configurations (open and short circuit) is rather small [0.5-0.35] in comparison with [0.6-0.2] for the square section at $\theta_0 = 0°$.

4.3. Effect of the reduced velocity at the best load resistance

Based on the best load resistance for each case, new tests are performed by varying the wind velocity. The records are triggered once the stability of LCO is observed, usually after more than 60 s of duration of the transient regime. Efficiencies and LCO amplitudes are shown Fig. 10 for the square section and Fig. 11 for the rectangular section. Note that these results are consistent with the ones presented in the previous section, especially in terms of the amplitude of the LCO.

We note that the square section at $\theta_0 = 10°$ is much more efficient than at $\theta_0 = 0°$. This can be explained by the corresponding LCO amplitudes and critical velocities. At $\theta_0 = 10°$ the critical velocity is lower than at $\theta_0 = 0°$ and this makes the section still oscillating for low velocities at $\theta_0 = 10°$ while simultaneously the galloping vanishes at $\theta_0 = 0°$. The square section at $\theta_0 = 10°$ is therefore a good candidate for the energy harvesting since its efficiency is always larger than the one obtained for $\theta_0 = 0°$. While some analytical studies (Barrero-Gil et al., 2010) found an optimal reduced velocity which maximizes the efficiency, it is not possible here to confirm, nor deny, the existence of such an optimal reduced velocity with the result obtained with the square section at $\theta_0 = 0°$.

The efficiency measured with the rectangular section is comparable to that measured with the square section at $\theta_0 = 0°$ with a maximum value around 0.02%. However, results show that after a sharp increase of the efficiency with the reduced velocity, a maximum value is reached close to $U_r = 140$. Beyond this reduced velocity the global efficiency decreases and the amplitude of oscillations still increases but in a weaker manner. There is clearly an optimal value of the reduced velocity for this section, while the results found with the square section do not allow to find an optimal velocity.
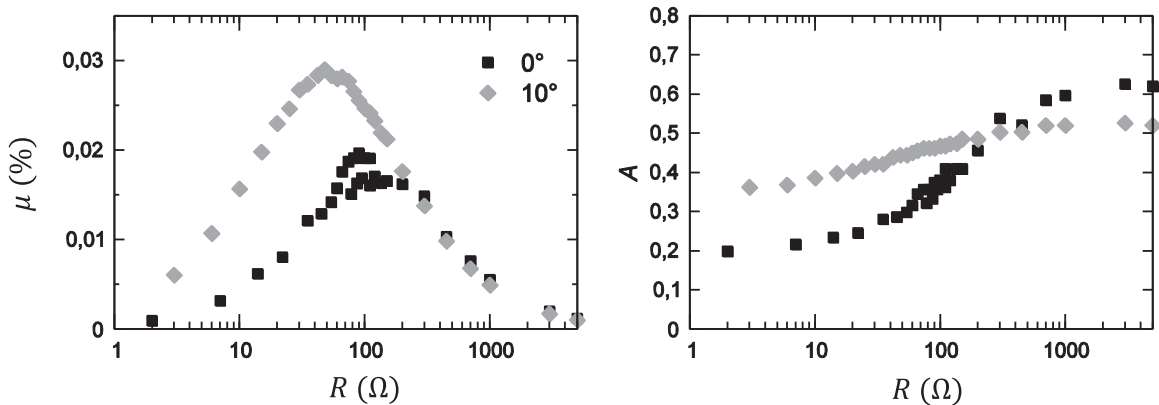

Fig. 8. Energy harvesting results for the square section at the constant reduced velocity $U_r = 88$ (left: efficiency, right: non dimensional amplitude).
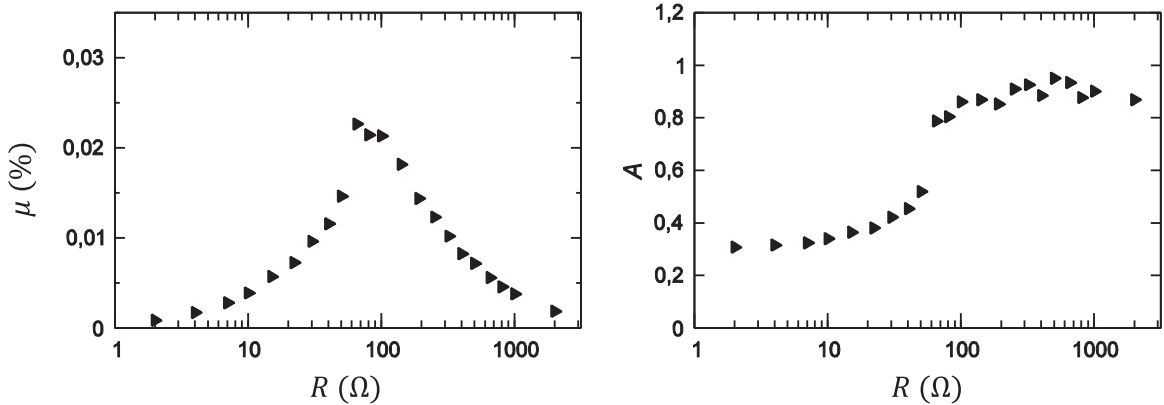
Fig. 9. Energy harvesting results for the rectangular section at the constant reduced velocity U_r=141 (left: efficiency, right: non dimensional amplitude).

5. Discussion

5.1. Considerations about the design of the coil/magnet assembly

Fig. 12 shows the magnets motion and the resulting voltage measured through the coil with time. In this figure, the sketches of the magnets and the coil are scaled according to the vertical axis on the left side. The magnets reach the outside of the coil twice per cycle (upper and lower positions of the magnets). The voltage generated by the coil being proportional to the time variation of the magnetic flux passing through it, it results in a double frequency of that of the magnet motion.

This figure sheds light on important considerations about the design of the harvesting system. The diameter of the coil should be adapted to the amplitude of the structural motion due to galloping. The frequency of the motion is also important as it impacts the magnetic flux variation and hence the amplitude of the resulting voltage. As stated previously, the resistance of the coil is also important and must be adapted to the one of the load resistance. Finally the number of turns and the inductance value, has also a proportional impact on the voltage. All these design parameters can certainly be improved by a specific study.

Vicente proposed a simple electromechanical model of the aeroelastic system coupled with an RL circuit (Vicente-Ludlam at al, 2014).

$$M\,(\ddot{Z}+2\eta\omega\dot{Z}+\omega^2 Z)=F_Z-k_E i.\quad (R+R_L)i+L\frac{di}{dt}=k_E\frac{dZ}{dt}.$$

(12)

using the electromechanical coefficient k_E and i the electric current. Assuming a harmonic behaviour, k_E can be computed as:

$$k_E=\frac{V_{RMS}}{Z_{RMS}}\frac{(1+R_L/R)}{\omega}\sqrt{1+\beta^2}$$

(13)

in which the parameter $\beta = L\omega/R + R_L$ characterises the ratio between the electrical and mechanical time periods.

Using the previous measurements it is possible to quantify the value of the electromechanical coupling as a function of the amplitude of mechanical oscillations. Results are reported in Fig. 13 where it is shown that k_E is almost constant with a mean value of 1.1. In comparison Vicente-Ludlam et al. (2014) identified a value of k_E equal to 10.6. It can be concluded that our harvesting device induces a weaker coupling with the galloping system.
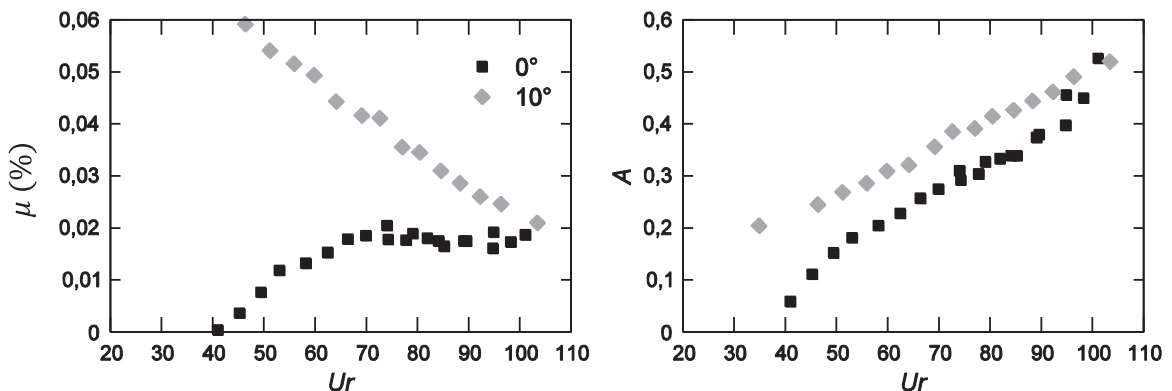

Fig. 10. Energy harvesting results for the square section at the best load resistance, R=90 Ω for θ_0=0° and R=50 Ω for θ_0=10° (left: efficiency, right: non dimensional amplitude).
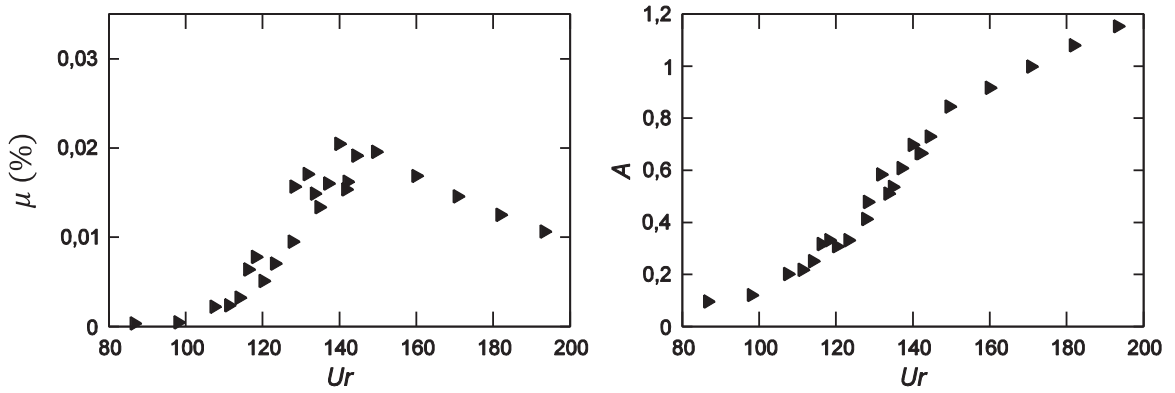
Fig. 11. Energy harvesting results for the rectangular section at the best load resistance $R=80\,\Omega$ (left: efficiency, right: non dimensional amplitude).
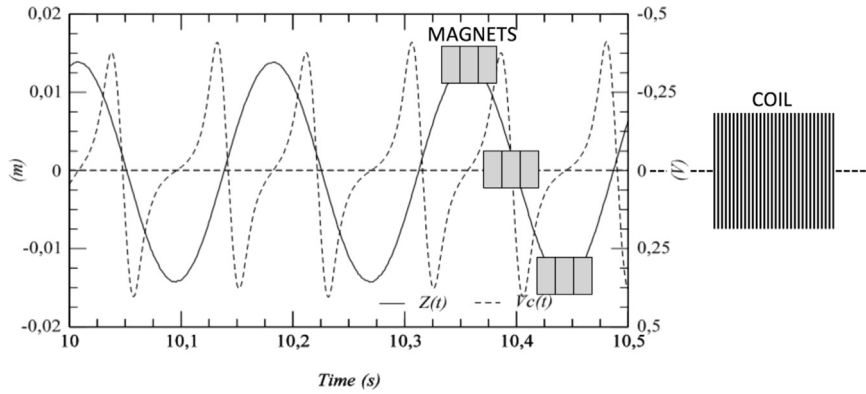

Fig. 12. Sample time histories of the magnet displacement $Z(t)$ and voltage $V(t)$ for $Ur = 100.5$ and $R = 80\,\Omega$.

In the present study $\beta \ll 1$, which means that the effect of the inductance on the dynamic response is negligible (Vicente-Ludlam et al., 2014). As a consequence the electromechanical force can be seen as an additional damping which can be written as a reduced electromechanical damping

$$\eta_E = \frac{k_E^2}{2 \quad \omega M \quad (R + R_L)}.$$

(14)

For the square section at $\theta_0=10°$ and $R = 48\,\Omega$, we obtain $\eta_E=0.056\%$ to compare with the structural damping $\eta = 0.19\%$ or the aerodynamic damping

$$\eta_a = \frac{\rho D S U}{4 M \omega} \left(\frac{dC_z}{d\theta} \right)_{\theta=\theta_0},$$
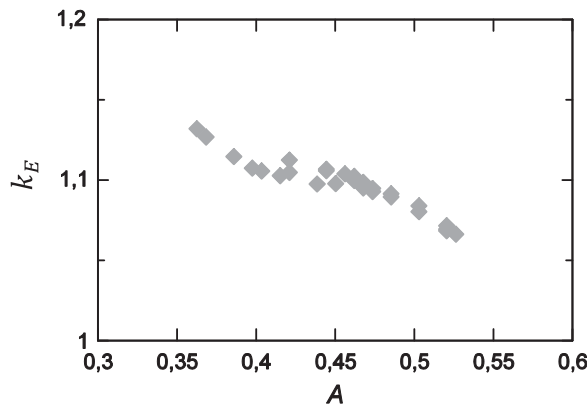
(15)

Fig. 13. Coupling coefficient k_E computed from the measurements with the square section at $\theta_0=10°$ and $U_r=88$ (as shown in Fig. 7).

which is worth $\eta_a = -0.28\%$ at $U_r = 88$. The equivalent electromechanical damping is then rather small compared to the structural and added aerodynamic damping. It means that a small energy extraction leads to the optimal efficiency. This is consistent with the very low efficiency values that have been found.

5.2. About the efficiencies

Another efficiency definition may be of interest for the physical interpretations of the measurements presented in this study. Indeed, galloping oscillations are due to the aerodynamic damping and energy harvesting can be performed only from this mechanism. Starting from the linear equation of motion (5) a characteristic value of the power that can be harvested is defined as

$$P_g = \frac{1}{T}\int_0^T \left(-\frac{1}{2}\rho DSU\left(\frac{dC_z}{d\theta}\right)_{\theta=\theta_0} - 2\ M\omega\eta\right)\dot{Z}^2 dt.$$
(16)

Assuming a periodic motion such as $Z(t) = \sqrt{2}Z_{RMS}\sin\omega t$ we can compute analytically the previous expression so that

$$P_g = \left(-\frac{1}{2}\rho DSU\left(\frac{dC_z}{d\theta}\right)_{\theta=\theta_0} - 2\ M\omega\eta\right)\omega^2 Z_{RMS}^2.$$
(17)

This power can be computed from the measurements of the LCO amplitude Z_{RMS} and the parameters of the prisms given in Tables 1 and 2. Then the global efficiency can be expressed as the product of two components, an efficiency of the galloping behaviour times the efficiency of the mechanical-electrical conversion

$$\frac{P_e}{P_w} = \frac{P_g}{P_w}\frac{P_e}{P_g}.$$
(18)

The first ratio in (18) is interesting in the sense that it is independent from the electrical production system: it should be the first quantity to analyse in order to choose the best configuration of prism galloping. Remember that the expression above comes from a linear equation and the decomposition (18) of the efficiency in two terms is used only to discuss the experimental results. For this reason it cannot be used as a predictive tool. However, the non-linear features of the system are taken into account through the measured LCO amplitudes. The ratio of galloping power to wind power can be written as

$$\frac{P_g}{P_w} = \frac{A^2}{1+2A}\frac{4}{U_r^2}\frac{\pi^2}{}\left(-\left(\frac{dC_z}{d\theta}\right)_{\theta=\theta_0} - \frac{4\pi S_c}{U_r}\right).$$
(19)

Introducing the critical velocity (7) in its non-dimensional form, relation (19) can also be expressed as

$$\frac{P_g}{P_w} = -\frac{A^2}{1+2A}\frac{16}{U_r^2}\frac{\pi^3 S_c}{}\left(\frac{1}{U_r} - \frac{1}{U_{rc}}\right).$$
(20)

This "galloping" efficiency is shown in Fig. 14 for the square section, together with the harvester system efficiency P_e/P_g and in Fig. 15 for the rectangular section.

Note that the small value of the global efficiency P_e/P_w observed in Section 4 is due to the small power available in the galloping phenomenon, as the ratio P_g/P_w always remains below 0.3% in all the tested cases. Concerning the efficiency of the harvesting system, which compares the electrical power to the power available from galloping, relatively good values are found: 12% for the rectangular section and up to 25% for the $\theta_0 = 0°$ configuration. One can also notice that the associated optimal load resistances are significantly lower than for the global efficiency. Despite the extreme simplicity of the electro-mechanical setup, its efficiency proves to be good and could even be optimized by a further specific study.
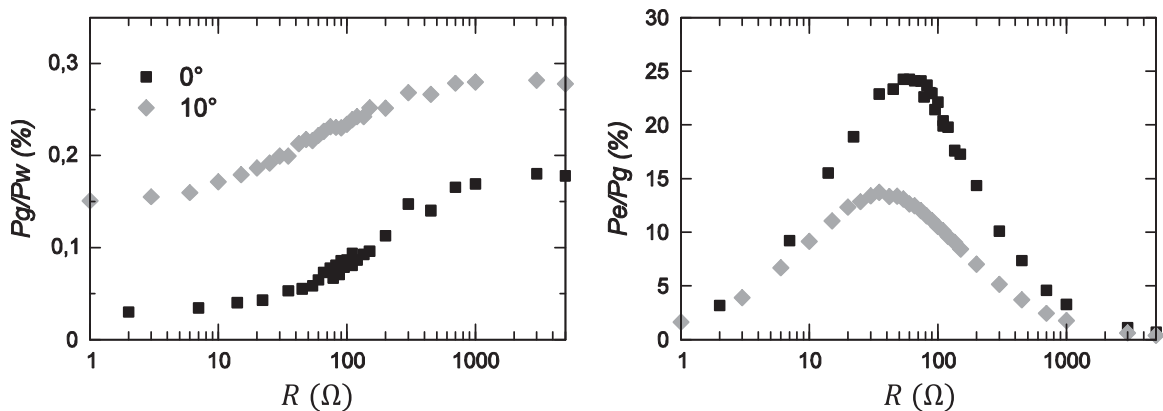

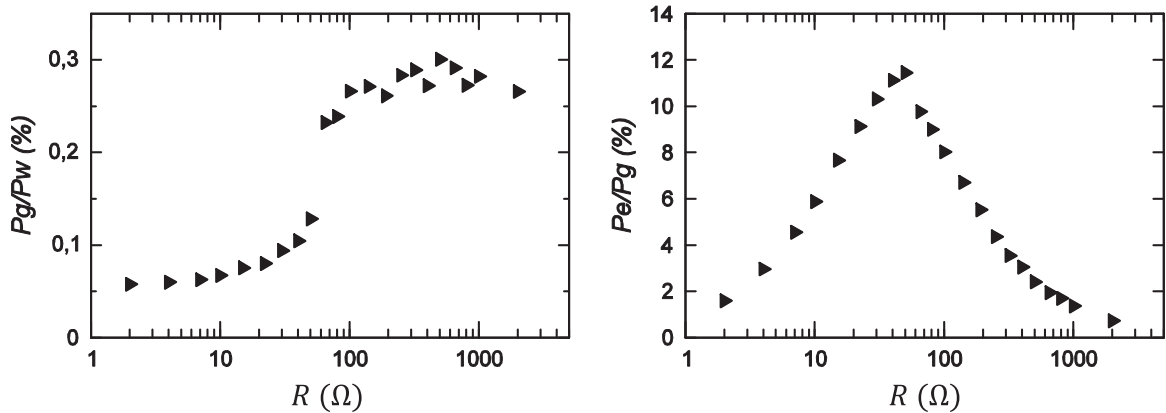**Fig. 14.** Efficiencies components for the square section at $U_r = 88$.

Fig. 15. Efficiencies components for the rectangular section at $U_r=141$.

Nevertheless, by comparison with the analytical study of Vicente-Ludlam et al. (2014), the efficiencies found experimentally here are considerably lower. Two reasons, at least, can be given: firstly the definition of the efficiency is different since we use the surface swept by the prism, by using the LCO amplitude, while they use the prism width alone. Secondly, Vicente-Ludlam et al. searched optimal conditions for harvesting energy based on an efficiency definition that is referred to a wind power which is independent of LCO amplitude. For the DD-section they considered, the amplitudes corresponding to the optimal efficiencies were indeed considerably larger and a bit unrealistic on an engineering point of view. Therefore and especially in the context of large amplitude of oscillations, it seems more convenient to work with a definition of the efficiency based on the effective surface swept by the system.

6. Conclusions

Galloping of prisms was investigated experimentally in a wind tunnel in order to estimate the potential of this mechanism for producing electric power from wind. The tested configurations were chosen from preliminary observations and with the stability of the LCO as the decisive criterion. A square section at $\theta_0=0°$ and at $\theta_0=10°$ and a 2/3 section at $\theta_0=2°$ have been selected. A simple energy harvester was designed. It consists in magnets located on the moving prism in front of a coil-core at rest. Efficiency of the system is found very small compared to standard wind turbine due to the galloping mechanism physics. However the electromechanical setup converting translating motion in electric energy is interesting and could certainly be improved.

Experimental investigations show also that two optimal load resistances exist, one linked to the galloping mechanism and another one linked to the energy converter. When the setup is designed so that these optimal resistances are joined, it can lead to the best efficiency of such a system. The square section at $\theta_0=10°$ presented in the paper is probably close to this optimal design but further tests with other working conditions are necessary to confirm this feature.

Although efficiency of this "prism wind turbine" is rather low, it remains interesting to further investigations and optimization because of its extreme simplicity and cost. Moreover such kind of system can be developed at various scales, for water current or wind and, thanks to the noiseless functioning due to the low frequency of the oscillations, it can be placed in a number of situations where standard wind turbines cannot.

References

Abdelkefi, A., Hajj, M., R., Nayfeh, A., H., 2013. Piezoelectric energy harvesting from transverse galloping of bluff bodies. Smart Mater. Struct. 22, 015014.

Andrianne, T., Dimitriadis, G., 2014. Empirical modelling of the bifurcation behaviour of a bridge deck undergoing across-wind galloping. J. Wind Eng. Ind. Aerodyn. 135, 129–135.

Barrero-Gil, A., Alonso, G., Sanz-Andres, A., 2010. Energy harvesting from transverse galloping. J. Sound Vib. 329, 2873–2883.

Barrero-Gil, A., Sanz-Andrés, A., Alonso, G., 2009. Hysteresis in transverse galloping: the role of inflection points. J. Fluids Struct. 20, 1007–1020.

Blevins, R.D., 2001. Flow-Induced Vibrations. Krieger Publishing Company, Malabar, Florida, (Reprint of the 1990s edition).

Carassale, L., Freda, A., Marrè-Brunenghi, M., 2013. Effects of free-stream turbulence and corner shape on the galloping instability of square cylinders. J. Wind Eng. Ind. Aerodyn. 123, 274–280.

Den Hartog, J.P., 1985. Mechanical Vibrations. Dover, New York, Reprint of the 1934 edition.

Ewere, F., Wang, G., Cain, B., 2014. Experimental investigation of galloping piezoelectric energy harvesters with square bluff bodies. Smart Mater. Struct. 23, 104012.

Hémon, P., 2012. Large galloping oscillations of a square section cylinder in wind tunnel. Flow-Induced Vibrations, FIV2012, Dublin, Ireland, July 3–6.

Kiwata, T., Nakajima, A., Mizukami, S., Ueno, T., Kono, T., 2016. Effect of angle of attack on vibration characteristics of a cantilevered prism for energy harvest. In: Proceedings of the First International Symposium on Flutter and its Application, Tokyo, 15–17 May, Paper ISFA-5R02.

Luo, S.C., Chew, Y.T., Ng, Y.T., 2003. Hysteresis phenomenon in the galloping oscillation of a square cylinder. J. Fluids Struct. 18, 103–118.

Mannini, C., Marra, A.M., Bartoli, G., 2014. VIV–galloping instability of rectangular cylinders: review and new experiments. J. Wind Eng. Ind. Aerodyn. 132, 109–124.

Michelin, S., Doaré, O., 2013. Energy harvesting efficiency of piezoelectric flags in axial flows. J. Fluid Mech. 714, 489–504.

Ng, Y.T., Luo, S.C., Chew, Y.T., 2005. On using high-order polynomial curve fits in the quasi-steady theory for square-cylinder galloping. J. Fluids Struct. 20, 141–146.

Norberg, C., 1993. Flow around rectangular cylinders: pressure forces and wake frequencies. J. Wind Eng. Ind. Aerodyn. 49, 187–196.

Novak, M., 1969. Aeroelastic galloping of prismatic bodies. J. Eng. Mech. Div. ASCE 96, 115–142.

Novak, M., 1971. Galloping and vortex induced oscillations of structures. In: Proceedings of the 3rd International Conference on Wind Effects on Buildings and Structures. Shuppan Co. Ltd, 799–809.

Novak, M., 1972. Galloping oscillations of prismatic structures. J. Eng. Mech. Div. ASCE 98, 27–46.

Novak, M., Tanaka, H., 1974. Effect of turbulence on galloping instability. J. Eng. Mech. Div. ASCE 100, 27–47.

Parkinson, G.V., Brooks, N.P.H., 1961. On the aeroelastic instability of bluff cylinders. ASME J. Appl. Mech. 1961, 252–258.

Parkinson, G.V., Smith, J.D., 1964. The square prim as an aeroelastic non-linear oscillator. Q. J. Mech. Appl. Math. XVII, 225–239.

Parkinson, G.V., 1989. Phenomena and modelling of flow-induced vibrations of bluff bodies. Prog. Aerosp. Sci. 26 (2), 169–224.

Païdoussis, M.P., Price, S.J., De Langre, E., 2011. Fluid-Structure Interactions: Cross-Flow Induced Instabilities. Cambridge University Press, Cambridge, UK.

Saathoff, P., Melbourne, W.H., 1999. Effects of freestream turbulence on streamwise pressure measured on a square-section cylinder. J. Wind Eng. Ind. Aerodyn. 79, 61–78.

Sousa, V.C., Anicezio, M. de M., De Marqui, C., Jr., Erturket, A., 2011. Enhanced aeroelastic energy harvesting by exploiting combined nonlinearities: theory and experiment. Smart Mater. Struct., 20. http://dx.doi.org/10.1088/0964-1726/20/9/094007.

Vicente-Ludlam, D., Barrero-Gil, A., Velazquez, A., 2014. Optimal electromagnetic energy extraction from transverse galloping. J. Fluids Struct. 51, 281–291.